Chapter 6

Quartz Tuning Fork Based Low Temperature Atomic Force Microscopy

6.1 Introduction

The invention of scanning tunneling microscopy (STM) in 1982[1] and atomic force microscopy (AFM) in 1986[2] has enabled people to "see" atoms on solid surfaces, which is important to the understanding of surface microscopic structures and their relationship to both surface and bulk electronic and mechanical properties. Although AFM has a relatively lower resolution when compared to STM, the advantage of probing both conducting and non-conducting materials makes AFM a very popular tool in the surface science community.[3, 4] Over the past two decades, various efforts have been made to improve both the resolution and throughput of the AFM technique.[5] This includes sensor design in both static and dynamic AFM operation modes.

In static mode, a cantilever probe is brought to the surface and the deflection due to the sample-tip interactions is monitored via a laser detection system (Figure 6.1, left). The interaction force is thereby straightforwardly obtained from Hooke's law. The surface topography is mapped out by raster scanning the probe while controlling the distance via a feedback system to maintain a constant interaction force. Thus a three-

dimensional image z(x, y, F_{ts} ≈ constant) is created, where z is height and the sample surface stays in the x-y plane. The early report of "atomic" resolution of the periodic lattice of NaCl(001) was obtained using this technique.[6]

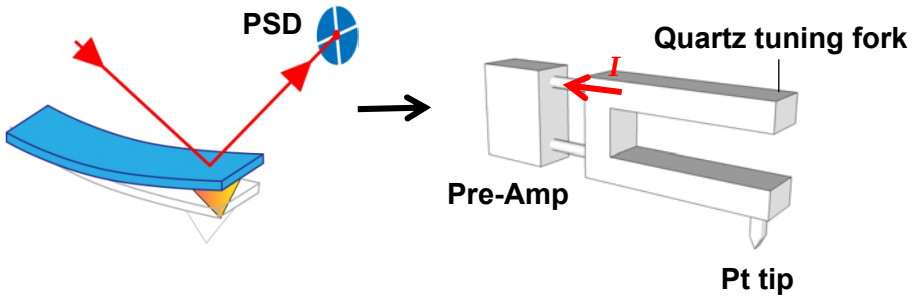

Figure 6.1. A schematic of AFM detection systems. Left, laser detection system. The tip-sample interaction force is sensed by the readout of the position changes of the laser spot through a photo sensitive diode (PSD). Right, quartz-tuning-fork-force-sensor detection system. The tip-sample interaction force is transduced to electric signals through the piezoelectric effect of quartz, which is then sensed by a pre-amplifier.

However, static AFM suffers from several problems. First, low stiffness (0.01-1 N m^{-1}) cantilever has to be used in order to increase the sensing of the force. This relatively soft cantilever is easily subject to thermal drifts. It is then rather difficult for the feedback system to maintain a constant interaction force during image acquisition. Furthermore, since the cantilever stiffness (k_c) is very low, a jump-to-contact instability occurs whenever the maximum interaction force gradient ($k_{ts} = \left| dF_{ts}/dz \right|$) exceeds k_c. This usually crashes an initially sharp tip and interferes with the feedback signal. In static contact mode, the image resolution is limited to the tip-surface contact radius (>10 nm). Most often, many "minitips" would be in contact with the surface and the resolution is typically >10 nm. It is also worthwhile to mention that since the tip is moved laterally in

contact, the relatively large interaction force would be detrimental to samples, in particular soft bio-samples.

In order to overcome the accompanying problems with static AFM, dynamic operation mode was developed in the past decade, which led to a significant transformation of AFM.[5] Dynamic AFM has been emerging as a powerful and versatile technique for atomic and nanometer-scale characterization and manipulation of a variety of surfaces. High-resolution images of DNA, proteins and polymers have been obtained in air and liquids.[7]

Basically, dynamic AFM uses a vibrating cantilever instead of a static one. The vibration of the cantilever is typically monitored by the laser detection system. Changes of the vibration amplitude or frequency due to the tip-sample interaction force are used as feedback signal to control the tip positions. A thorough understanding of the tip motion dynamics is then critical for the understanding of the feedback mechanism, detection sensitivity and improvement of resolution.

Usually, a harmonic approximation is used to describe the dynamics of the tip with damping.[5] In this approximation, the cantilever-tip ensemble is modeled as a harmonic oscillator with effective mass m* and spring constant k_c. If we assume the average distance between the tip and sample surface is z_0 (see Figure 6.2), and the deflection of the cantilever from its equilibrium position is z, the instantaneous position of the tip relative to the surface is then z_0+z.

The equation of motion for the tip is then

$$m^{*}\ddot{z} + k_c z + \frac{m\omega_0}{Q_0}\dot{z} = F_{ts} + F_0\cos(\omega t) \tag{6.1}$$

in which F_0 and ω are the amplitude and angular frequency of the exciting force exerted by the driving piezo on the cantilever. Q_0, ω_0 and k_c are the quality factor, free angular resonance frequency and force gradient of the cantilever-tip ensemble, respectively.

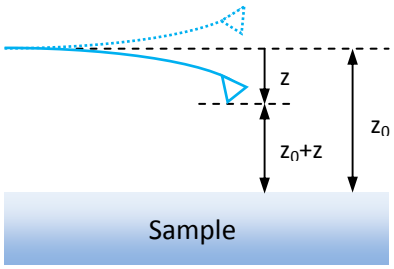

Figure 6.2. A scheme of the relevant spatial distances in dynamic AFM. The instantaneous position of the tip is defined with respect to the average position of the tip. The up deflection of the cantilever is defined to be positive z.[5]

Hence, in the absence of interaction force, Eq. (6.1) describes the motion of a forced harmonic oscillator with damping. This will generally give a solution of both static and transient states. Solving this equation with $F_{ts} = 0$ and ignoring the transient solution, the free amplitude of vibration as a function of frequency is obtained by the Lorenztian expression[5]

$$A(\omega) = \frac{F_0/m}{[(\omega_0^2 - \omega^2)^2 + (\omega\omega_0/Q_0)^2]^{1/2}} \tag{6.2}$$

and the phase shift by

$$\tan\varphi = \frac{\omega\omega_0/Q_0}{\omega_0^2 - \omega^2} \tag{6.3}$$

where φ, the phase shift, is the angle by which the driving force leads the deflection of cantilever. When the tip is brought to the proximity of the surface, the interaction force will modify the vibration of the tip. The force acting on the tip is a complicated function of tip-sample distance $F_{ts}(d = z+z_0)$. Generally, there is no analytical solution for Eq. (6.1). Applying a small-amplitude approximation, in which the force can be written as

$$F_{ts}(d) = F(z_0) - k_{ts} z \tag{6.4}$$

where k_{ts} is force gradient evaluated at the equilibrium position z_0 of the tip. Thus Eq. (6.2) becomes

$$A(\omega) = \frac{F_0 / m}{[(\omega_e^2 - \omega^2)^2 + (\omega\omega_e / Q(z_0))^2]^{1/2}} \tag{6.5}$$

where the effective resonance frequency is calculated by

$$\omega_e = \sqrt{(k_c + k_{ts}) / m^*} \tag{6.6}$$

and the quality factor becomes a function of the average distance z_0 between tip and sample,

$$Q(z_0) = Q_0 \frac{\omega_e}{\omega_0} \tag{6.7}$$

assuming the damping coefficient γ is constant within a whole tip vibrating cycle.

Therefore, due to a change of the resonance frequency from ω_0 to ω_e, the amplitude and phase shift are then expected from Eqs. (6.2) and (6.3). These three parameter changes then can be used as feedback control to keep the tip in a constant

equilibrium position relative to the sample atoms. Based on different feedback mechanisms, dynamic AFM technique includes two major types: amplitude modulation atomic force microscopy (AM-AFM) and frequency modulation atomic force microscopy (FM-AFM).

In AM-AFM, the cantilever-tip ensemble is vibrated at a constant frequency, which is the same of or near its free resonance frequency. The oscillation amplitude is used as a feedback control to measure the surface topography. Most of the AM-AFM experiments are performed in air or in liquids.[5] Although considerable achievements have been made by using this technique, attaining true atomic resolution image still encounters significant problems. Firstly, since AM-AFM tends to use a large oscillation amplitude (10-100 nm) and a relative stiff (of the order of a few 10 N/m) cantilever, the small amplitude approximation is not applicable. The analysis of the tip dynamics is complicated by several factors. The force gradient would vary considerably during a vibration cycle and induce nonlinear features in the dynamics of the tip motion. Several dissipative processes, such as surface adhesion hysteresis, viscoelasticity and electronic dissipation would be involved in the tip motion. Secondly, an intrinsic bi-stable state exists for the AM-AFM operation. This bi-stable state refers to the existence of two amplitude values with respect to a fixed frequency, and is due to the co-existence of attractive and repulsive forces between tip and sample surface. Therefore, it interferes with the amplitude feedback and causes instabilities during acquisition process. Additionally, AM-AFM is rarely used in ultrahigh vacuum (UHV) environment, although the UHV system may potentially boost the detection sensitivity. This is because the relatively high quality factor of the cantilever in vacuum will extend the lifetime (τ =

$2Q_0/\omega_0$) of the transient state of the tip motion, and result in a delay in amplitude feedback response.

Fortunately, most of the above-mentioned problems can be largely avoided by employing FM-AFM, which was invented by Albrecht and colleagues in 1991 for magnetic force microscopy.[8] In FM-AFM, the cantilever-tip ensemble is vibrated at its resonance frequency ω_e at all times. This is achieved by phase shifting the deflection signal and feeding it back to the piezo actuator which drives the cantilever. By scanning a cantilever across the sample (in the x-y plane) and adjusting z such that the frequency shift is constant, a map $z(x, y, \Delta\omega \approx \text{constant})$ is created.

By using a large amplitude (34 nm), a true atomic resolution image of the reactive Si(111)-(7×7) reconstruction surface was first obtained in UHV by Giessibl in 1995.[9] Since then a number of studies on conductive and insulating surfaces have been performed by using FM-AFM.[10] It has been found that the amplitude should be large when compared to the range of F_{ts} to attain optimal resolution:[11] jump-to-contact would still occur if a relatively small amplitude were used instead. On the other hand, the use of large amplitudes (>10 nm) is not comparable to the short range of chemical bonds, which have a range of ~1 Å. Therefore, a better understanding of the frequency shift with respect to the tip-sample interaction would be expected to provide insights to the choice of parameters in order to improve the sensitivity and resolution.

Giessibl et al.[12] have shown that reduced noise would be expected if we used small oscillation amplitude. By modeling the tip-sample interaction force as an

exponential function of the tip-sample distance, the vertical noise δz was derived as follows:[12]

$$\delta z \propto \frac{\left(1+\sqrt{\frac{\pi}{2}}\left(\frac{A}{\lambda}\right)^{3/2}\right)}{A}\sqrt{TB} \tag{6.8}$$

where λ, T and B is the interaction force range, temperature, and detection bandwidth. According to Eq. (6.8), a minimal noise is expected when A ≈ λ (Å range) and the product of temperature and bandwidth is minimized. However operation with such very small amplitudes is not possible with conventional cantilevers due to the instabilities caused by jump-to-contact and perturbations of the oscillation by tip-sample dissipation. To overcome these problems, a cantilever with rather large stiffness (more than 1000 N/m) is required.

Because the commercial silicon cantilevers cannot afford such high stiffness, a piezoelectric quartz tuning fork usually used in watch industry (Fig. 6.1, right) has been used instead by researchers.[13-17] In addition, instead of the conventional laser-PSD detection scheme, the vibration of the quartz tuning fork can be directly monitored electronically, as the mechanical vibration of the tuning fork is transduced to electric signals through the piezoelectric effect of quartz, which is then detected by a pre-amplifier. High-resolution images have been obtained at room temperature by Giessibl et al.[18, 19] Additionally, when compared to silicon cantilevers, the relative frequency shift with respect to temperature is rather small for quartz tuning forks, which results in an enhanced stability of the force sensor. These studies show the potential application of quartz tuning forks in AFM imaging. However, the construction of quartz-tuning-fork-

based AFM systems suitable for low-temperature measurements remains challenging. This is because silicon-based pre-amplifiers were used to sense the vibration of the quartz tuning forks in previous studies,[18-20] but silicon-based amplifiers are not functional at cryogenic temperatures due to carrier freeze-out. To carry out cryogenic (~ 4 K) temperature experiments with such systems, in previous attempts a thermal shield box was used to house the electronics.[21, 22] However, the close proximity of the box to the force sensor induces mechanical coupling to the tuning fork. Furthermore, heavy liquid helium consumption is expected due to the relatively high temperature inside the box (~ -40ºC).

In this chapter, we investigated the mechanical properties of quartz-tuning-fork-based force sensor and integrated it into a low-temperature AFM system. The optical detection scheme will be replaced by a home-made electronics design. A GaAs field effect transistor (FET)-based pre-amplifier, which functions at cryogenic temperatures, will be designed and coupled to the force sensor. Our goal is to construct a quartz tuning fork-based high-speed, high-resolution FM-AFM system applicable to especially low temperature and UHV environments. In Section 6.2, we outline the methods to design the pre-amplifier, the setup of the low-noise detection system and the assembly of the tuning-fork-tip ensemble. Noise and quality factor performance of the designed electronics, as well as feasibility of the force sensor, will be discussed in Section 6.3.1 and 6.3.2. The preliminary experiments on silicon surfaces will be discussed in Section 6.3.3. Conclusions will be presented in Section 6.4.

6.2 Experimental

6.2.1 Pre-amplifier

In the present study, a GaAs FET-based pre-amplifier was used instead of the conventional silicon-based circuits, since carrier freeze-out would not occur for GaAs at cryogenic temperatures. The circuit consists of a first-stage pre-amplifier and a second-stage op amp (see Fig 6.5). The first-stage preamplifier is put in the low temperature environment for the AFM test, while the second-stage op amp stays at room temperature.

The circuit was built on a copper-covered circuit board. Briefly, a designed electronic circuit was transferred to the covered copper using a conventional method followed by lift-off of the exposed copper by ferric chloride solution. Special care was taken to avoid wire crossing and ground loops, with a common ground being used throughout on the circuit board. The electronic units (op amps, resistors and capacitors) were then connected to the wires on the other side of the board. Since generally most of the noise comes from the first-stage amplifier,[23] the resistors used in this stage were metal film type with a relatively small thermal noise level and carbon resistors were used in other parts of the circuit instead.

Low-noise high-gain heterojunction GaAs MESFETs were used in this work for the first-stage amplifier. We choose three brands for comparison purposes: EPB018A5 from Excelics, ATF-35143-BLK from Agilent Technologies and FHX13X(14X,45X) from Fujitsu. Since the accumulation of static charge on the gate capacitor would induce a breakdown gate-to-source voltage, protective diodes were also used.

The op amp with large gain and wide bandwidth was preferred in the present design. We chose an OPA602 amplifier from Burr-Brown as the second stage. Several other types of op amps were also tested, such as OPA111 and OP27.

6.2.2 Low noise measurements

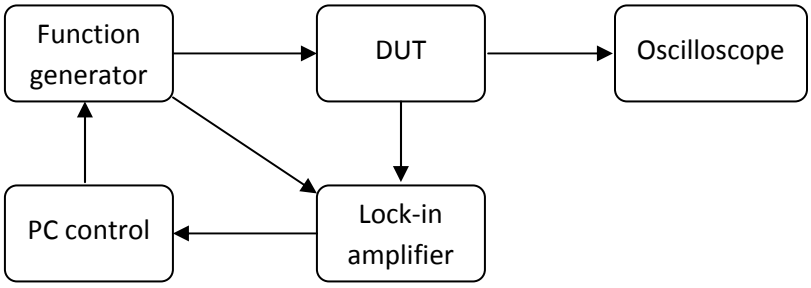

Figure 6.3. A schematic of the low-noise detection system.

The low-noise detection system was performed by using a lock-in amplifier (Figure 6.3). To evaluate the noise performance of the device under test (DUT), an alternating voltage signal was triggered by the function generator and fed to the DUT. A synchronized reference signal was sent to the Lock-in amplifier, which is used to test the noise level at various reference frequencies. The output of the DUT was connected to the input of Lock-in amplifier. The control of frequency tuning, measurement of output signal from DUT and tuning of reference frequency in Lock-in were realized through GPIB connection to a computer. A program written with Labview 6.1 was used to control the operations. Additionally, an oscilloscope was also connected to the DUT when necessary to monitor the signal and noise levels. To minimize the noise level induced by the different ground connections, the ground line from all the instruments including the DUT were connected to a common ground point.

The function generator used in this paper was a DS360 model from Stanford Research Systems. It exhibits a steady 25 ppm frequency stability and the frequency range is from 10 mHz to 200 kHz. The noise level of this generator is < -100 dBc. The low-distortion property enables us to use a sine wave with a small voltage of 4 μV (root mean square, rms) to excite the tuning fork.

Noise level detection was performed by using a SR830 DSP Lock-in amplifier (Stanford Research Systems). The time constant and slope used in the experiments is 300 ms and 12 dB, respectively. The oscilloscope was HP 54520A model from Hewlett Packard and was used as a monitor to adjust the offset potential at the converting terminal of the op amp. Additionally, it is also used in the evaluation of the amplifier gain.

To evaluate the noise performance at cryogenic temperature (~ 4 K), a cryostat of Model STVP-100 from Janis was used. The low temperature was obtained by injecting liquid helium into the chamber inside the cryostat. The temperature was monitored with a thermometer of Model 330 from Lakeshore. The circuit board was mounted on the end of a long rod equipped with the cryostat. Although the long rod may induce some mechanical vibration, which could be coupled to the circuit, the frequency of this vibration is rather low and so this coupling effect can be ignored. The temperature sensor (silicon diodes) was also attached to the end of the metal rod and in close proximity to the circuit board.

6.2.3 Tuning-fork-tip assembly

The quartz tuning fork used in this paper was from ECS Company. The free resonance frequency f_{bare} = 32.768 kHz, and the spring constant is over 1000 N/m. The Q-factor is about 90,000 in a sealed state. The temperature stability is -0.04 ppm / ºC.

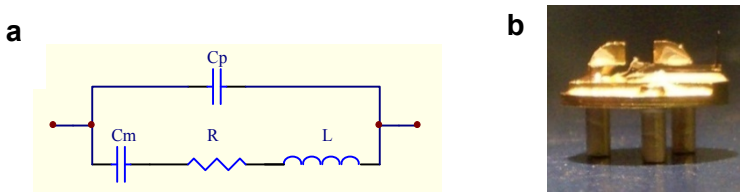

Figure 6.4. Quartz-tuning-fork-tip assembly. (a) Equivalent circuit of a tuning fork. (b) An optical image of the quartz-tuning-fork-tip assembly. One prong of the quartz tuning fork is glued to the tip holder. The Pt-Ir tip (appearing black) is glued perpendicularly to the other prong of the tuning fork.

The piezoelectric quartz tuning fork can be viewed as a parallel connection of the shunt capacitance C_p and motional units, C_m, R, L (inductor) as shown in Figure 6.4a. The series resonance corresponds to the cancellation of the impedance from the motional capacitor and that of the inductor, indicating a minimum of the absolute impedance value. The vibrational frequency of the quartz tuning fork is thus transduced into the electrical resonance frequency of the equivalent circuit. This resonance is used in the present study and the frequency shift due to the tip-sample interaction is used as a feedback signal to control the tip-sample separations.

The force sensor is made by attaching a tungsten tip to the end of the prong (Figure 6.4b). Silver paint was used so that the tip was electrically connected to one of

the electrodes of tuning fork. The connection of the electrodes to the pre-amplifier circuit is realized by using an ultrathin Au wire with a diameter of 12 μm. This is to minimize the stress applied to the tuning fork.

6.3 Results

6.3.1 Noise performance

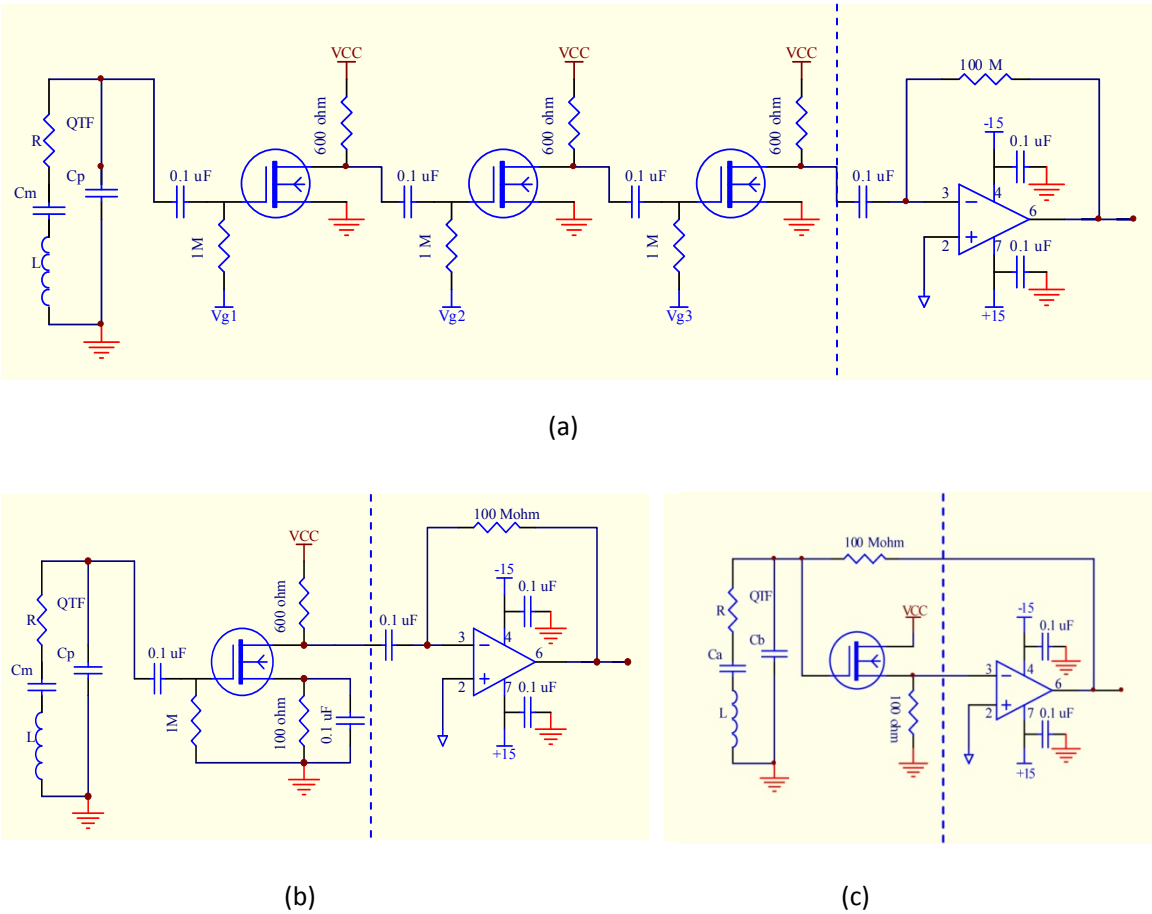

(a)

(b)

(c)

Figure 6.5. Low noise detection scheme. A schematic of three types of electronic circuits for low-noise detection of signal from tuning fork: (a) common-source, (b) self-biasing and (c) global feedback. Each of the circuits consists of a first-stage (left to the dashed line) pre-amplifier and a second-stage op amp (right of the dashed line).

Three types of pre-amplifiers: common-source, self-biasing and global feedback have been designed in this study, as shown in Figure 6.5a-c.

As mentioned previously, each of the circuits consists of a first-stage (left of the dashed line) pre-amplifier and a second-stage op amp (right of the dashed line). The first-stage pre-amplifier is put in the low-temperature environment for AFM test, while the second-stage op amp stays at room temperature. The GaAs MESFET used in the first stage is of n-type depletion mode. The op amp serves as the second stage for further amplification. As we know, the use of long thin wires at cryogenic temperature usually leads to a high (resistance-capacitance) time constant, which reduces the bandwidth of the amplifier.[24] More importantly, the use of long connection wire will cause a significant degradation of signal from the tuning fork with a high impedance (over 35 kΩ), because the impedance of the wire and tuning fork does not match. Therefore, in our design the input terminal of the first-stage preamplifier was placed as close as possible to the electrodes of the tuning fork.

As mentioned above, the noise induced from the first stage is critical to the overall noise performance, hence the parameters associated with this stage were optimized to obtain a minimized noise floor. Typical values of the resistors, capacitor and voltages were indicated in Figure 6.5. For instance, in common-source type, increase of the drain resistor value would increase both voltage gain and noise level. An optimal value of ~600 Ω was obtained in our experiment.

Table 6.1. Comparison of noise floor at room temperature for three types of amplifiers: common source, self-biasing and global feedback. The unit is μV $Hz^{-1/2}$

Common-source	Self-biasing	Global feedback
~ 13	~ 9	~ 1

The tuning fork can be either mechanically or thermally excited. In this experiment, the thermally activated tuning fork was used to evaluate the noise performance of the designed electronics so that no extra noise from the actuator was induced. It was found that little or no resonance signals were obtained for the common source and self-biasing amplifiers. Typical noise spectral density values at ~32768 Hz (resonance frequency of the tuning fork) are summarized in Table 6.1, where the noise floor for the global feedback is the lowest. The relatively noisier performance of the former two circuits likely overwhelmed the weak thermally activated resonant signals.

Figure 6.6a compared the noise performance for the global feedback with an op-amp-only amplifier circuit, which was used by Giessibl et al.[25] The corresponding circuits were also shown in Figure 6.6b. The experiments were performed at room temperature. It can be seen from the figure that these two circuits have a comparable noise floor and thermal activated signal can be observed for both. The resonance curve peaks at about 32764.8 Hz. Corresponding low-temperature (4.18 K) experiments showed that this peak shifted to 32711.5 Hz and a narrower sharp resonance peak was obtained (not shown here).

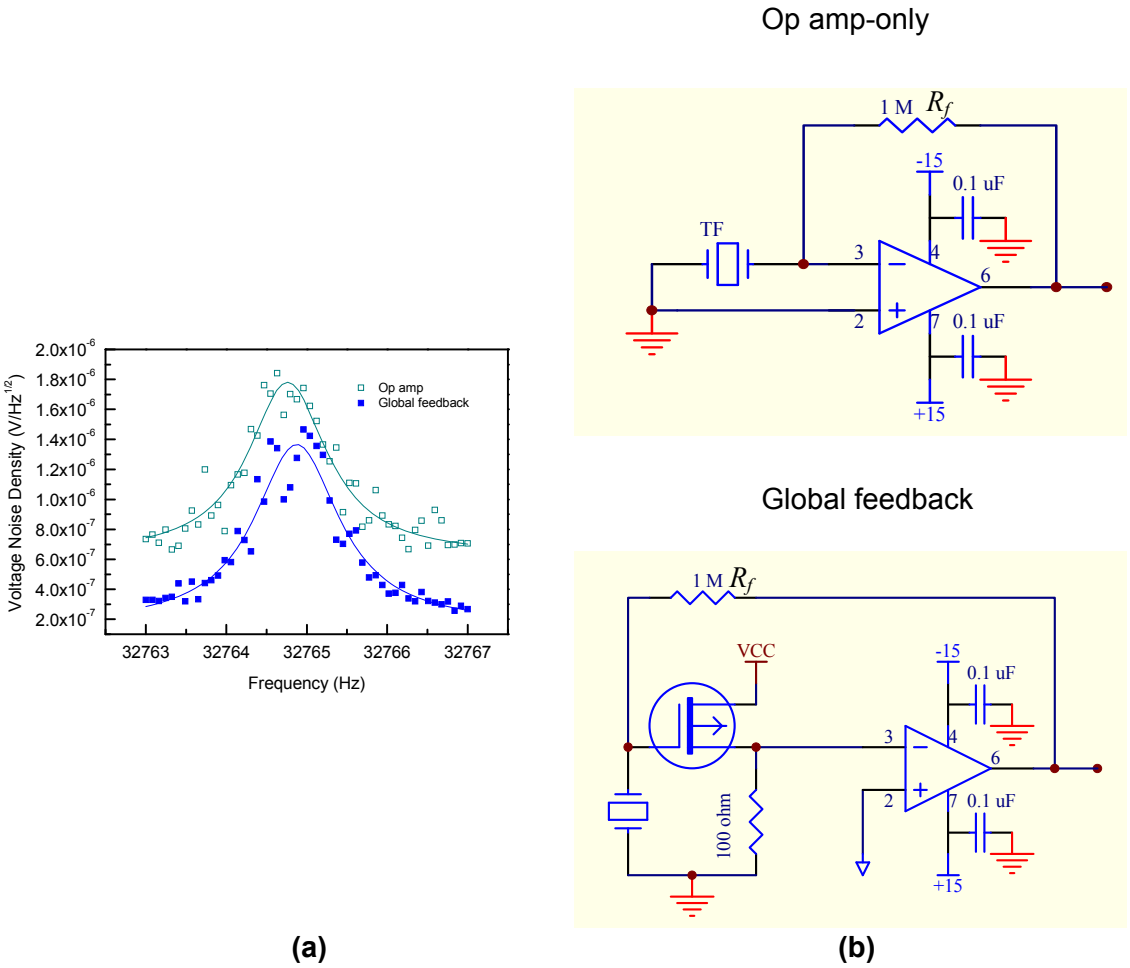

Figure 6.6. Noise performance. (a) Comparison of the noise spectral density for the op-amp-only and global feedback pre-amplifiers at room temperature; (b) Corresponding circuits for the two pre-amplifiers.

The sensitivity of the pre-amplifier (defined as V_{out}/z) can be determined experimentally and theoretically. According to the studies by Giessibl,[20] the sensitivity can be written as

$$S(f) = 24\pi f G d_{21} k_c L_e (L_e/2 - L)/t^2 \tag{6.9}$$

where f, L_e, L, t are resonance frequency, tuning fork beam electrode length, beam length and beam thickness, respectively. d_{21} (= 2.31 $\times 10^{-12}$ C/N) is the coupling constant for quartz. G is the trans-impedance gain of the pre-amplifier. For op-amp only, $G = -R_f$ and for global feedback, the transfer function can be derived as[24]

$$G = \frac{V_{out}(\omega)}{I_{in}(\omega)} = -R_f \left[\frac{G_1(\omega)G_2(\omega)}{1 + G_1(\omega)G_2(\omega)} \right] \tag{6.10}$$

where R_f is the feedback resistor (see Figure 6.6b), and $G_1(\omega)$ and $G_2(\omega)$ are the voltage gain for the first- and second-stage global feedback amplifier. Since the op amp gain is usually far larger than that of the FET, G of the global feedback can be approximately $-R_f$ too. Using Eqs. (6.9) and (6.10), we obtained a sensitivity of 0.95 μV/pm for both circuits when R_f = 1 MΩ for both.

The sensitivity can also be obtained from Figure 6.6a. The output voltage is obtained by integrating over the resonance curve, subtracting that from the noise floor. The thermal noise amplitude was calculated to be about 1.2 and 1.3 μV for op-amp-only and global feedback circuits, respectively. The r.m.s. thermal vibration amplitude (A_{th}) is calculated from $k_c A_{th}^2 = k_B T$, where k_B is the Boltzmann constant. For room temperature (T = 293 K), A_{th} = 1.49 pm. Then the sensitivity is 0.81 and 0.87 μV/pm for op-amp-only and global feedback circuits, respectively.

The above study showed that at room temperature, the GaAs-based global feedback pre-amplifier can provide a good sensitivity comparable to the silicon-based op-amp-only amplifier, which enables the detection of even signal from a thermally activated tuning fork.

6.3.2 Quality factor

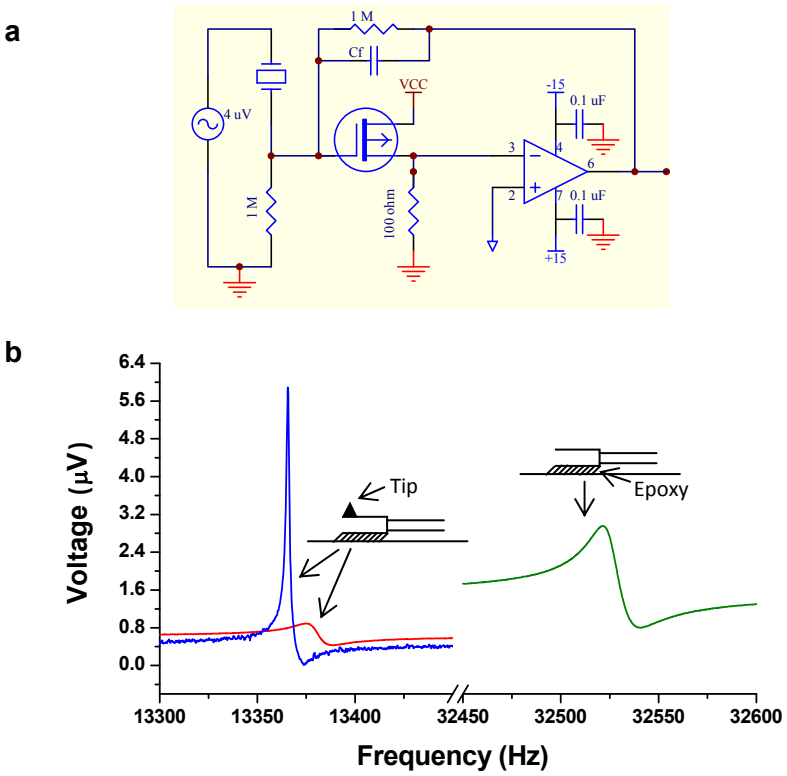

Figure 6.7. Excitation curves for quality-factor measurements. (a) Circuit (global feedback type) for external excitation experiments. (b) Excitation curves for a q-Plus type tip-tuning fork assembly sensor. Green, one prong is attached to the substrate and the curve is acquired at room temperature in air. Red, same as green except that the other prong is attached with a tip (filled triangle). Blue, same as red except the setup is in vacuum and the temperature is 77 K. The excitation voltage is 4 μV.

A high quality-factor (Q-factor) of the tuning-fork-tip ensemble is required for accurate detection of the frequency shift in FM-AFM. The Q-factor is examined by using an external excitation source. Figure 6.7a showed the circuit, where an extra resistor was connected in parallel with the tuning fork.

We examined the Q-factor for the q-Plus sensor (Figure 6.4b). Figure 6.7b showed the corresponding frequency response to the excitation. The Q-factor drops from ~30,000 (commercial) to ~900 due to the large damping effect of the epoxy. As a Pt-Ir tip is glued to the other prong of the tuning fork, resonance frequency shifted from 32521 Hz to 13375 Hz due to the extra mass added to the prong. Meanwhile, the Q-factor further drops to ~200. When in vacuum, the slight increases in both resonance frequency and Q-factor were observed (data not shown here). A large increase in Q-factor (~ 9000) is observed when the temperature is dropped to ~77 K (Figure 6.7b, blue line).

6.3.3 Topographic images

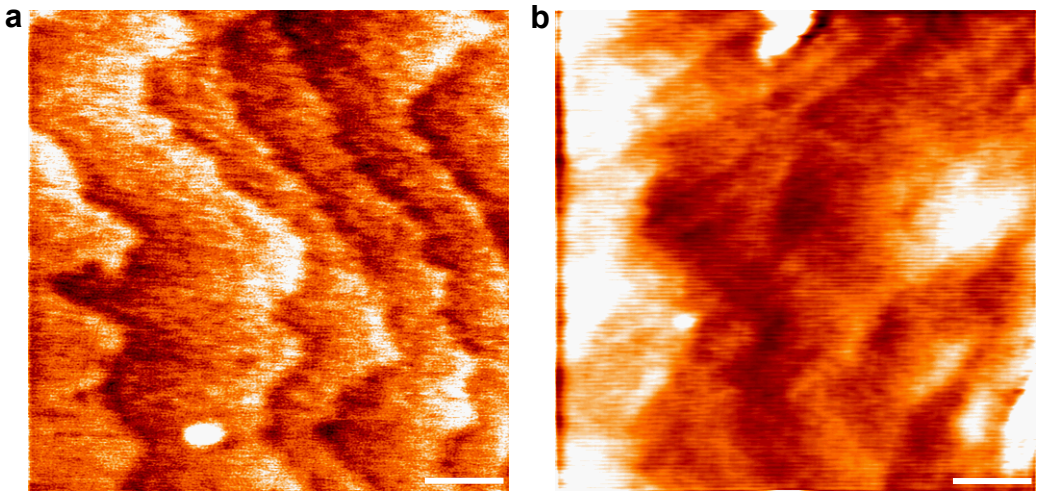

Figure 6.8. Frequency-modulated AFM topographic images. (a) H-terminated Si(111) at room temperature. (b) The same sample at liquid nitrogen temperature (77K). The set point is 20 Hz. The scale bar is 100nm. Vertical scale is from 0 to 2 nm.

Figure 6.8a shows typical frequency-modulated AFM topographic images of H-terminated Si(111) surfaces at room and liquid nitrogen temperature (77K), respectively.

This verifies our design of quartz-tuning-fork-based force sensor and pre-amplifier. The terrace and steps of at least one atomic height (~3.15 Å) are clearly seen on the images. However, the image resolution still needs to be improved in the future work. This may include optimization of the pre-amplifier design in order to further decrease the noise level; application of proper epoxy to minimize the damping of the q-Plus force sensor, etc.

6.4 Conclusion

In this chapter, the electronics functional at cryogenic temperatures to detect the signal from a quartz tuning fork has been designed. This force-sensor-electronic-detector system has been employed in frequency-modulated atomic force microscopy (FM-AFM). Noise performance of three types of pre-amplifier electronics has been compared. Results show that the force-sensor-global-feedback circuit detector system induces the lowest noise floor. The high detection sensitivity of this system demonstrates its ability to be used in FM-AFM at cryogenic temperatures. The quality factor of the tuning-fork-tip ensemble has also been examined. We found that a high Q of ~9000 in vacuum at ~77K is obtained for a q-Plus tuning-fork-tip ensemble system. This facilitates accurate detection of frequency in AFM operation. Surface topographic imaging from H-terminated Si(111) surfaces has been achieved, which verifies our rational design of quartz-tuning-fork-based force sensor and pre-amplifier.

6.5 References

1. Binning, G., Rohrer, H., Gerber, C. & Weibel, E. Surface studies by scanning tunneling microscopy. *Phys Rev Lett* **49**, 57-61 (1982).
2. Binnig, G., Quate, C.F. & Gerber, C. Atomic force microscope. *Phys Rev Lett* **56**, 930-933 (1986).

3. Morita, S., Wiesendanger, R., Meyer, E. & Giessibl, F.J. Noncontact atomic force microscopy. (Springer, Berlin; New York; 2002).
4. Giessibl, F.J. & Quate, C.F. Exploring the nanoworld with atomic force microscopy. *Phys Today* **59**, 44-50 (2006).
5. Garcia, R. & Perez, R. Dynamic atomic force microscopy methods. *Surf Sci Rep* **47**, 197-301 (2002).
6. Meyer, G. & Amer, N.M. Optical-beam-deflection atomic force microscopy - the NaCl (001) surface. *Appl Phys Lett* **56**, 2100-2101 (1990).
7. Bustamante, C. & Keller, D. Scanning force microscopy in biology. *Phys Today* **48**, 32-38 (1995).
8. Albrecht, T.R., Grutter, P., Horne, D. & Rugar, D. Frequency-modulation detection using high-Q cantilevers for enhanced force microscope sensitivity. *J Appl Phys* **69**, 668-673 (1991).
9. Giessibl, F.J. Atomic-resolution of the silicon (111)-(7x7) surface by atomic-force microscopy. *Science* **267**, 68-71 (1995).
10. Sugawara, Y., Ohta, M., Ueyama, H. & Morita, S. Defect motion on an InP(110) surface observed with noncontact atomic-force microscopy. *Science* **270**, 1646-1648 (1995).
11. Giessibl, F.J. Forces and frequency shifts in atomic-resolution dynamic-force microscopy. *Phys Rev B* **56**, 16010-16015 (1997).
12. Giessibl, F.J., Bielefeldt, H., Hembacher, S. & Mannhart, J. Imaging of atomic orbitals with the Atomic Force Microscope - experiments and simulations. *Ann Phys-Berlin* **10**, 887-910 (2001).
13. Giessibl, F.J. Advances in atomic force microscopy. *Rev Mod Phys* **75**, 949-983 (2003).
14. King, G.M. & Nunes, G. Attractive-mode force microscope for investigations of biomolecules under ambient conditions. *Rev Sci Instrum* **72**, 4261-4265 (2001).
15. Patil, N.G. & Levy, J. Low-noise variable-temperature preamplifier for piezoelectric tuning fork force sensors. *Rev Sci Instrum* **73**, 486-487 (2002).
16. Urazhdin, S., Tessmer, S.H. & Ashoori, R.C. A simple low-dissipation amplifier for cryogenic scanning tunneling microscopy. *Rev Sci Instrum* **73**, 310-312 (2002).
17. Jahncke, C.L., Brandt, O., Fellows, K.E. & Hallen, H.D. Choosing a preamplifier for tuning fork signal detection in scanning force microscopy. *Rev Sci Instrum* **75**, 2759-2761 (2004).
18. Giessibl, F.J. Atomic resolution on Si(111)-(7x7) by noncontact atomic force microscopy with a force sensor based on a quartz tuning fork. *Appl Phys Lett* **76**, 1470-1472 (2000).

19. Giessibl, F.J., Hembacher, S., Bielefeldt, H. & Mannhart, J. Subatomic features on the silicon (111)-(7x7) surface observed by atomic force microscopy. *Science* **289**, 422-425 (2000).

20. Giessibl, F.J. High-speed force sensor for force microscopy and profilometry utilizing a quartz tuning fork. *Appl Phys Lett* **73**, 3956-3958 (1998).

21. Hembacher, S., Giessibl, F.J. & Mannhart, J. Evaluation of a force sensor based on a quartz tuning fork for operation at low temperatures and ultrahigh vacuum. *Appl Surf Sci* **188**, 445-449 (2002).

22. Giessibl, F.J., Hembacher, S., Herz, M., Schiller, C. & Mannhart, J. Stability considerations and implementation of cantilevers allowing dynamic force microscopy with optimal resolution: the qPlus sensor. *Nanotechnology* **15**, S79-S86 (2004).

23. Motchenbacher, C.D. & Connelly, J.A. Low-noise electronic system design. (Wiley, New York; 1993).

24. Yang, C.H., Chang, T.H., Yang, M.J. & Moore, W.J. A low noise transimpedance amplifier for cryogenically cooled quartz tuning fork force sensors. *Rev Sci Instrum* **73**, 2713-2716 (2002).

25. Hembacher, S., Giessibl, F.J. & Mannhart, J. Force microscopy with light-atom probes. *Science* **305**, 380-383 (2004).